Dalton Transactions

Accepted Manuscript

This article can be cited before page numbers have been issued, to do this please use: R. Van Deun, A. M. Kaczmarek, K. Van Hecke, I. Van Driessche, M. D'hooge and A. Savic, *Dalton Trans.*, 2015, DOI: 10.1039/C5DT03147H.

This is an *Accepted Manuscript*, which has been through the Royal Society of Chemistry peer review process and has been accepted for publication.

Accepted Manuscripts are published online shortly after acceptance, before technical editing, formatting and proof reading. Using this free service, authors can make their results available to the community, in citable form, before we publish the edited article. We will replace this *Accepted Manuscript* with the edited and formatted *Advance Article* as soon as it is available.

You can find more information about *Accepted Manuscripts* in the Information for Authors.

Please note that technical editing may introduce minor changes to the text and/or graphics, which may alter content. The journal's standard Terms & Conditions and the Ethical guidelines still apply. In no event shall the Royal Society of Chemistry be held responsible for any errors or omissions in this *Accepted Manuscript* or any consequences arising from the use of any information it contains.

ROYAL SOCIETY OF CHEMISTRY

www.rsc.org/dalton

View Article Online
DOI: 10.1039/C5DT03147H

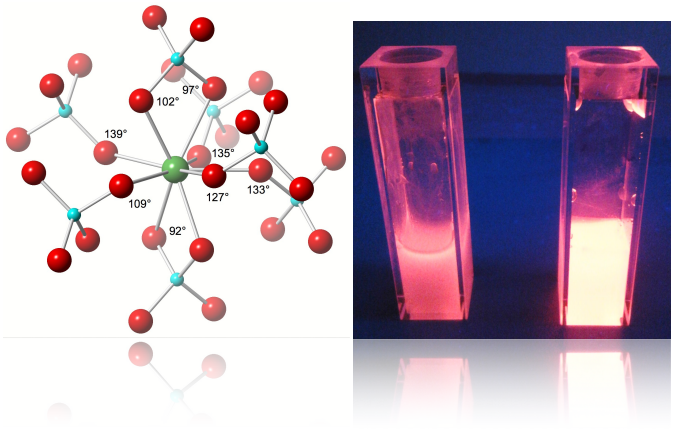

Enhancement of the luminescence properties of Eu^{3+} doped monoclinic $LaVO_4$ nanoparticles was investigated through co-doping with Y^{3+}, Gd^{3+} and Lu^{3+} ions.

ROYAL SOCIETY OF CHEMISTRY
View Article Online
DOI: 10.1039/C5DT03147H

Journal Name

ARTICLE

Influence of Y^{3+}, Gd^{3+}, and Lu^{3+} co-doping on the phase and luminescence properties of monoclinic Eu:$LaVO_4$ particles

Rik Van Deun,[a,*] Micheline D'hooge,[a] Aleksandar Savic,[a,b,c] Isabel Van Driessche,[d] Kristof Van Hecke,[b] Anna M. Kaczmarek[a,*]

Received 00th January 20xx,
Accepted 00th January 20xx

DOI: 10.1039/x0xx00000x

www.rsc.org/

Nano-sized particles of monoclinic-$LaVO_4$ were prepared in a short reaction time of 30 minutes by employing a microwave assisted hydrothermal synthesis in the presence of glycerol, which was used both as a solvent and structure-directing agent. The tetragonal-$LaVO_4$ is known to show strong luminescence properties when doped with Ln^{3+}, whereas the monoclinic-$LaVO_4$ is usually considered not suitable for luminescence and therefore luminescence properties of monoclinic-$LaVO_4$ doped with Ln^{3+} ions are seldom investigated. Due to the scarce amount of research on the topic of luminescence of Ln^{3+} doped monoclinic-$LaVO_4$ in this paper a detailed study of solid state luminescence properties, including quantum yields, of nano-sized monoclinic-$LaVO_4$ doped with different molar percentages of Eu^{3+} is presented. It was observed that the 12.5% Eu^{3+} doped sample showed the strongest luminescence properties. Additionally a study of the influence of different rare-earth ions (Y^{3+}, Gd^{3+}, Lu^{3+}) co-doped into the particles was performed in order to explore the potential of increasing the luminescence of these materials. Furthermore stable colloidal suspensions of the Eu^{3+} doped monoclinic-$LaVO_4$ nanoparticles showing strong red emission could be obtained.

1. Introduction

Various inorganic compounds doped with trivalent lanthanide ions have found applications for example in lighting and displays, for biological applications, lasers, catalysts, magnets, optical amplifiers, and polarizers.[1-6] The luminescence properties of trivalent lanthanides are among the most unique. They result from transitions within the partially filled 4f shell. These transitions are parity forbidden leading to low molar absorption coefficients and long luminescent lifetimes.[7]

Among these inorganic compounds rare-earth orthovanadates doped with lanthanide ions are a class of materials that has attracted lots of interest due to their applications as phosphors, catalysts, and laser host materials.[8-10] Especially lanthanide doped YVO_4 and $GdVO_4$ materials have been extensively studied.[11-14] It has been reported that nano-sized lanthanide doped rare-earth vanadates have higher luminescence efficiency than known commercial phosphors.[15] $LaVO_4$ materials of different size and shape have also been investigated.[16-20] Unlike YVO_4 and $GdVO_4$, which crystalize in a tetragonal zircon type structure, $LaVO_4$ can crystallize in two polymorphs – monoclinic (*m*-) monazite type and tetragonal (*t*-) zircon type (see Fig. 1).[21-22] With increasing ionic radius rare-earth ions show a preference towards crystallizing in a monazite type orthovanadate. La^{3+}, which has the largest ionic radius among all the trivalent rare-earth ions, forms a thermodynamically stable monazite type structure and a metastable zircon type structure (La^{3+} ions are too large for this structure). The *t*- zircon type $LaVO_4$ (space group $I4_1/amd$) has a similar structure to YVO_4 and $GdVO_4$. It is composed of alternating edge-sharing REO_8 (RE – rare earth) dodecahedra and VO_4 tetrahedra forming chains parallel to the *c*-axis. The *m*- monazite $LaVO_4$ (space group $P2_1/n$) consists of REO_9 polyhedra, which share edges with VO_4 tetrahedra along the *c*-axis. In literature it can be found that lanthanide doped *t*-$LaVO_4$ shows very good luminescence properties (yet as a metastable phase it is not suitable for many further applications), on the other hand *m*-$LaVO_4$ (stable phase) is not considered a suitable host for luminescence.[17,20] This can be

[a] L^3 – Luminescent Lanthanide Lab, Department of Inorganic and Physical Chemistry, Ghent University, Krijgslaan 281-S3, B-9000 Ghent, Belgium; corresponding email: anna.kaczmarek@ugent.be, rik.vandeun@ugent.be
[b] XStruct, Department of Inorganic and Physical Chemistry, Ghent University, Krijgslaan 281-S3, B-9000 Ghent, Belgium.
[c] Faculty of Chemistry, University of Belgrade, Studentski trg 12-16, 11000 Belgrade, Serbia.
[d] SCRiPTS, Department of Inorganic and Physical Chemistry, Ghent University, Krijgslaan 281-S3, B-9000 Ghent, Belgium.
Electronic Supplementary Information (ESI) available: additional XRD patterns, DRIFTS spectrum of glycerol, additional emission and excitation spectra, and decay curves of all materials. See DOI: 10.1039/x0xx00000x

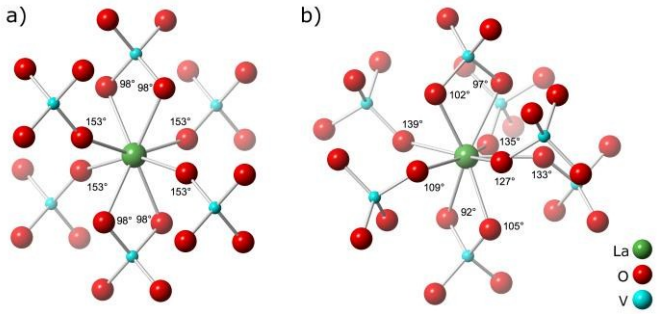

Fig. 1 Crystal structure of (a) tetragonal $LaVO_4$ and (b) monoclinic $LaVO_4$. The La-O-V angles (°) are indicated.

explained by the fact that in Ln^{3+} doped *m*-$LaVO_4$ for every lanthanide center there is only one Ln-O-V bond bridge with an angle suitable for wave functions of vanadium and the lanthanide to overlap, whereas in *t*-$LaVO_4$ there are four Ln-O-V bond bridges with a maximum angle of 153°. Here the σ bonds overlap effectively allowing efficient energy transfer. Unfortunately in the *m*-$LaVO_4$ the possibility of efficient energy transfer between the vanadium groups and Ln^{3+} ions is much less likely than in the *t*-$LaVO_4$. Because lanthanum is more abundant compared to other rare-earths it is a side product of the separation process to obtain other rare-earths, therefore La_2O_3 is much cheaper than most rare-earth oxides.[23] For this practical reason synthesizing lanthanum based host materials for efficient luminescence phosphors is highly desired.

In this study we have prepared nano-sized *m*-$LaVO_4$ in a fast microwave assisted hydrothermal synthesis carried out in the presence of glycerol. The motivation of the undertaken research was to explore the possibility of enhancing the luminescence properties of Eu^{3+} doped *m*-$LaVO_4$ through co-doping it with additional RE^{3+}. In all other known literature on this topic either Ln^{3+} doped *t*-$LaVO_4$ materials are investigated or Ln^{3+} doped *t*-$LaVO_4$ materials are only compared with Ln^{3+} doped *m*-$LaVO_4$ materials to show their superiority.
Emission and excitation spectra, luminescence lifetimes, and quantum yields of the samples at different Eu^{3+} doping and Y^{3+}, Gd^{3+}, and Lu^{3+} co-doping percentages were investigated both in the solid state and for stable colloidal suspensions.

2. Experimental Section

2.1. Synthesis

All chemicals (analytical grade) were purchased from Sigma Aldrich or VWR and used without further purification.

All samples were synthesized in a microwave assisted hydrothermal synthesis. First, 1 mmol of $Ln(NO_3)_3 \cdot 6H_2O$ (where Ln^{3+} = Y, La, Eu, Gd, Lu) was dissolved in 10 mL distilled water. To this a mixture of 20 mL glycerol dissolved in 10 mL distilled water was added. After several minutes a solution of 1 mmol Na_3VO_4 dissolved in 10 mL distilled water was added dropwise. The pH of the solution was adjusted to 4 by addition of diluted HNO_3. The solution was placed inside several 30 mL microwave furnace tubes, which were located in a microwave (CEM Discover SP with autosampler) and heated for 30 minutes at a temperature of 180 °C (200W, 20 bar, and no Powermax). The tubes were allowed to cool down naturally to room temperature. The precipitate was centrifugated (undoped samples: 7000 rpm for 5 minutes, doped samples: 9000 rpm for 10 minutes) and washed several times with water and then ethanol. The product was dried in a vacuum oven at 40 °C overnight. The samples were further heat treated at 900 °C for 3h to obtain the final products.

2.2. Characterization

XRD patterns were recorded by a Thermo Scientific ARL X'TRA diffractometer equipped with a Cu Kα (λ = 1.5405 Å) source, a goniometer and a Peltier cooled Si (Li) solid state detector. Chemical bonding was analyzed by infrared spectroscopy, using a Thermo Scientific FTIR spectrometer (type Nicolet 6700) equipped with a DRIFTS-cell. Samples were prepared by mixing the powders with KBr. The samples were measured in the 550-4000 cm^{-1} range. Particle shape and size were studied using SEM. SEM measurements were performed using a FEI Quanta 200 FSEM and an FEI Nova 600 Nanolab Dual-Beam focused ion beam in secondary electron mode.

The luminescence of solid samples and their colloidal suspensions in water (prepared by dispersing 0.01 g of the sample in 2 mL distilled water) was studied. Solid powdered samples were put between quartz plates (Starna cuvettes for powdered samples, type 20/C/Q/0.2). Colloidal suspensions were measured in quartz cuvettes with a pathlength of 10 mm. Luminescence measurements were performed on an Edinburgh Instruments FLSP920 UV-vis-NIR spectrometer setup. A 450W xenon lamp was used as the steady state excitation source. Luminescence decay times were recorded using a 60W pulsed Xe lamp, operating at a frequency of 100 Hz. A Hamamatsu R928P photomultiplier tube was used to detect the emission signals in the near UV to visible range. All of the luminescence measurements were recorded at room temperature. In order to compare the measurements the same amounts of powders were used as well as the same settings for each measurement (same slit size, step, and dwell time). All emission spectra in the manuscript have been corrected for detector response.
The luminescence decay curves of the samples were measured when excited into the maximum of the V-O charge transfer band and monitored at the appropriate wavelength. The decay curves could be well fitted using a single exponential equation (1):

$$I = I_0 \exp\left(-\frac{t}{\tau}\right) \quad (1)$$

where I and I_0 are the luminescence intensities at time t and 0, respectively, and τ is the luminescence lifetime. Absolute quantum yields of the heat treated samples were determined using an integrating sphere. Quantum yields were calculated using equation (2):

$$\eta = \frac{\int L_{emission}}{\int E_{blank} - \int E_{sample}} \quad (2)$$

View Article Online
DOI: 10.1039/C5DT03147H

where $L_{emission}$ is the integrated area under the emission spectrum, E_{blank} is the integrated area under the "excitation" band of the blank, and E_{sample} is the integrated area under the excitation band of the sample (as the sample absorbs part of the light, this area will be smaller than E_{blank}).

3. Results and discussion

3.1. Structure and morphology

The XRD patterns of samples obtained in a microwave assisted hydrothermal synthesis (at a pH of 4 in the presence of 20 mL glycerol) both before and after heat treatment could be well matched with the XRD pattern of monoclinic $LaVO_4$ calculated using the Mercury crystal structure visualization, exploration, and analysis tool.[24] Fig. 2 presents examples of XRD patterns showing the material before heat treatment and after heat treatment at 900 °C. Additionally the standard XRD patterns of monoclinic and tetragonal $LaVO_4$ are presented. Although the sample before heat treatment can be assigned to the monoclinic phase the crystallinity of the material significantly increased after heat treatment. No peaks of the tetragonal phase are present in either the samples before or after heat treatment. Increasing the pH to 6, different amounts of glycerol and also a shorter reaction time was shown to have a negative influence on the phase formation (supporting information Fig. S1). It was observed that doping the material with Eu^{3+} ions did not cause any changes in the XRD patterns. Although $EuVO_4$ crystallizes in a tetragonal phase, at a doping percentage of up to 15% Eu^{3+} ions no characteristic peaks of the tetragonal phase were observed. The XRD patterns of *m*-$LaVO_4$ doped with 2.5, 5, 10, 12.5, and 15% Eu^{3+} are presented in Fig. 3. In the XRD patterns of the doped samples it can be observed that the peaks become broader. It has been reported before that doping a material with additional ions can cause a size reduction, which will lead to broader peaks in the XRD diffractogram.[25] Due to the higher crystallinity of the heat treated samples, they were chosen for analyzing the luminescence properties.

To further characterize the materials DRIFTS spectra of the materials were recorded. Fig. 4 presents DRIFTS spectra of the *m*-$LaVO_4$ material before and after heat treatment. In both spectra a band around 950 cm^{-1} is present, which can be assigned to the V-O stretch vibrations. In the spectrum of the sample before heat treatment several additional bands are present. A band between 3400-3500 cm^{-1} can be attributed to the O-H vibrations from water and/or glycerol. Other peaks, which can be assigned to the C-H and O-H vibrations from glycerol are also present (see Fig. S2). This indicates that in the sample before heat treatment glycerol and water is present on the surface of the nanoparticles. After heat treatment at 900 °C all glycerol is burnt off and not present in the DRIFTS spectra.

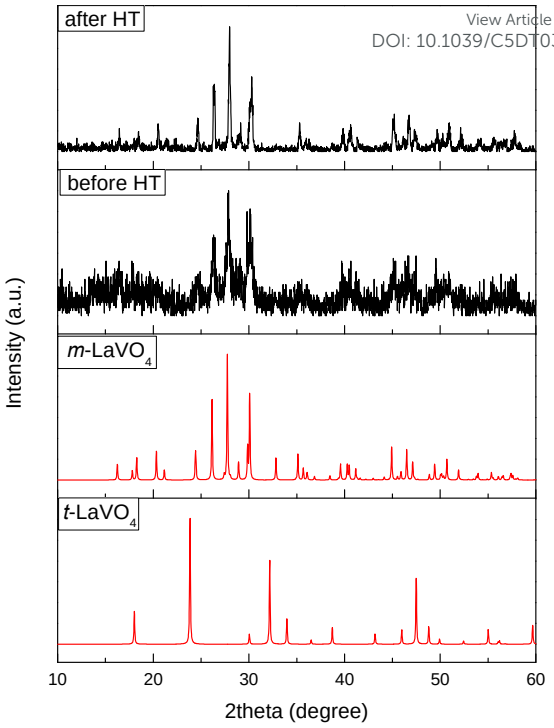

Fig. 2 XRD patterns of the $LaVO_4$ material before and after heat treatment at 900 °C. The standard XRD patterns of the monoclinic (*m*) and tetragonal (*t*) $LaVO_4$ are presented in red as reference.

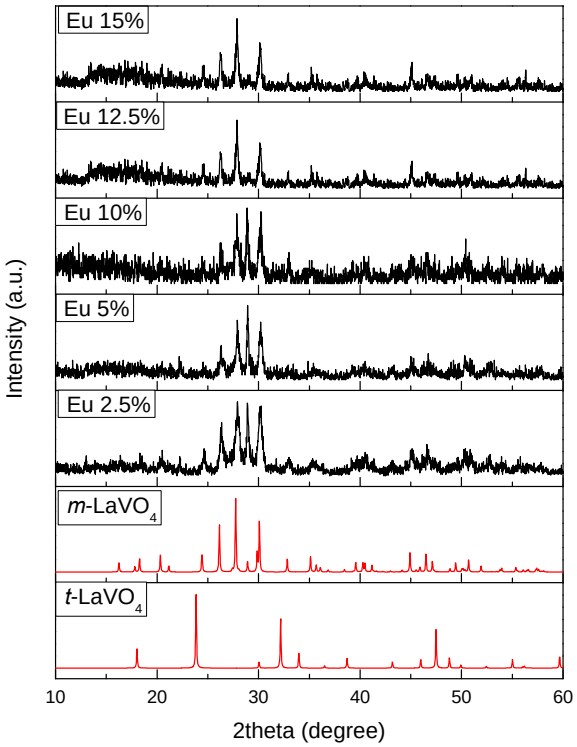

Fig. 3 XRD patterns of x% Eu:$LaVO_4$ (where x = 2.5, 5, 10, 12.5, and 15). The standard XRD patterns of the monoclinic and tetragonal $LaVO_4$ are presented in red as reference.

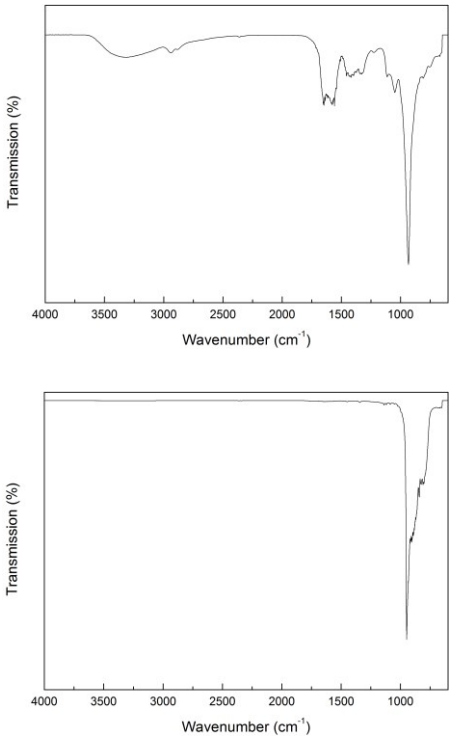

Fig. 4 DRIFTS spectra of the $LaVO_4$ material before (top) and after (bottom) heat treatment.

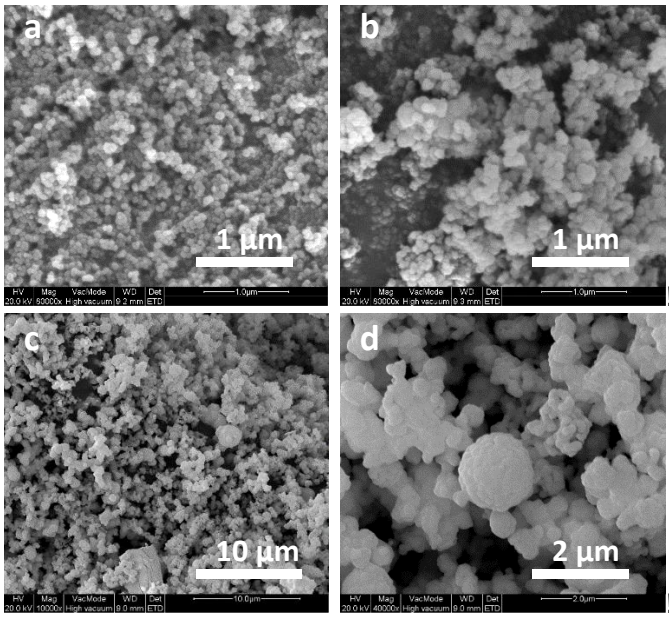

Fig. 5 SEM images of $LaVO_4$ material before (a,b) and after (c,d) heat treatment.

Last, the morphology of the samples was characterized by SEM, as presented in Fig. 5. In Fig. 5a,b the material before heat treatment is presented. Fig. 5c, d shows the material after heat treatment. Investigation of the morphology of Eu^{3+} doped particles showed a decrease in size compared to the undoped samples (see Fig 6). This is consistent with what was observed in the XRD patterns. This decrease in size after Eu^{3+} ion doping can mot likely be explained by the fact that after nucleation the Eu^{3+} ions are located at the surface of the particles inhibiting their further growth.[25-27]

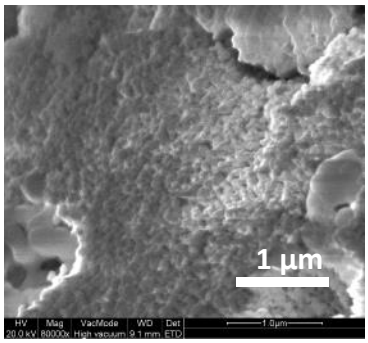

Fig. 6 SEM image of 10%Eu:$LaVO_4$ sample

3.2. Photoluminescence properties

Various rare-earth inorganic materials at the nano-size have been reported to be good host lattices for the luminescence of lanthanide ions. Among these materials also lanthanide doped rare-earth orthovanadates have shown to have very good luminescence properties. From an economical point of view lanthanum based host lattices are a good choice due to the low cost of lanthanum oxide compared to the other rare-earths. In this study monoclinic $LaVO_4$ nanoparticles doped with different percentages of Eu^{3+} ions were investigated in detail. The possibility of enhancing their luminescence through Y^{3+}, Gd^{3+} and Lu^{3+} co-doping was explored.

3.2.1. Photoluminescence properties of Eu^{3+} doped $LaVO_4$

Fig. 7 presents the room-temperature combined excitation-emission spectrum of 12.5%Eu:$LaVO_4$ material. In general for all of the Eu:$LaVO_4$ samples the excitation spectra consist of a strong broad band and several weaker sharp peaks. The maximum of the broad band is located around 316 nm. It is attributed to the vanadate groups. It corresponds to the charge-transfer absorption from the 2p orbitals of the oxygens to the 5d orbitals of vanadium. In line with the molecular orbital theory this corresponds to transitions from the $^1A_2(^1T_1)$ ground state to the $^1A_1(^1E)$ and $^1E(^1T_2)$ excited states of the vanadate groups (in crystalline $LaVO_4$ the original T_d symmetry of the vanadate ions is reduced to D_{2d} by the crystal field, and this causes a splitting of the degenerate levels of the vanadate groups).[14] The lower region of the broad band (around 280 nm) could also be attributed to the charge-transfer transition between the Eu^{3+} and O^{2-}.[28]

The weak sharp peaks can be assigned to the transitions of trivalent europium. In the emission spectra of Eu:$LaVO_4$ samples only the characteristic peaks of Eu^{3+} are present indicating an efficient transfer of energy from the V-O band to the Eu^{3+} ions. The peaks labeled in Fig. 7 have been assigned to the appropriate transitions in Table 1. The emission spectra of Eu:$LaVO_4$ samples with different doping concentrations are compared in Fig. 8. As can be observed the emission intensity

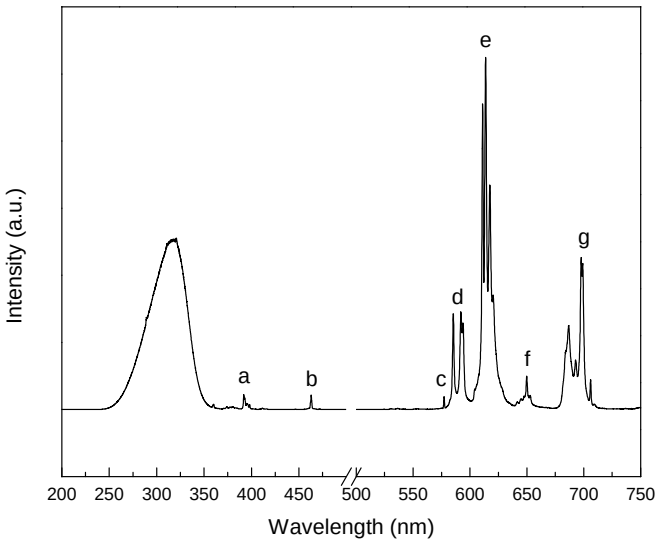

Fig. 7 Excitation spectrum (monitored at 613.2 nm) and emission spectrum (excited at 316.0 nm) of 12.5%Eu:$LaVO_4$ material. The electronic transitions labeled a-g are assigned in Table 1.

Table 1. Assignment of peaks labeled in Fig. 7

	Wavelength (nm)	Energy (cm^{-1})	Transition
Excitation			
a	391.5	25543	$^5L_6 \leftarrow {}^7F_0$
b	462.9	21603	$^5D_2 \leftarrow {}^7F_0$
Emission			
	Wavelength (nm)	Energy (cm^{-1})	Transition
c	577.5	17316	$^5D_0 \rightarrow {}^7F_0$
d	592.6	16875	$^5D_0 \rightarrow {}^7F_1$
e	613.2	16308	$^5D_0 \rightarrow {}^7F_2$
f	650.1	15382	$^5D_0 \rightarrow {}^7F_3$
g	697.7	14333	$^5D_0 \rightarrow {}^7F_4$

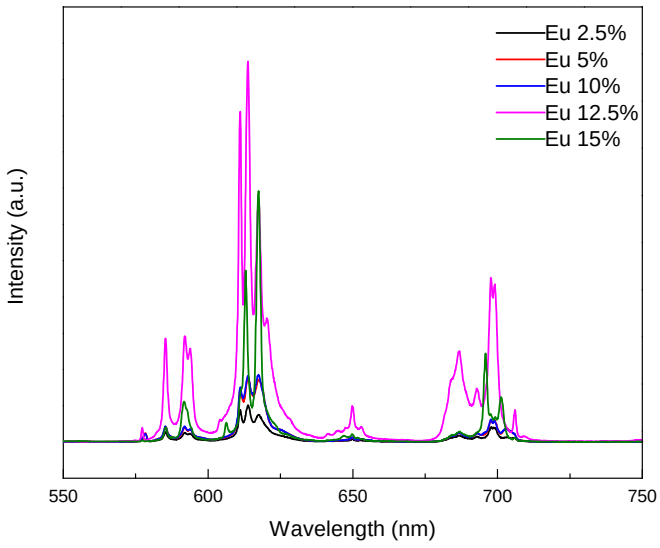

Fig. 8 Emission spectra of Eu^{3+}- (2.5%, 5%, 10%, 12.5% and 15%) doped $LaVO_4$ nanoparticles excited at 316.0 nm.

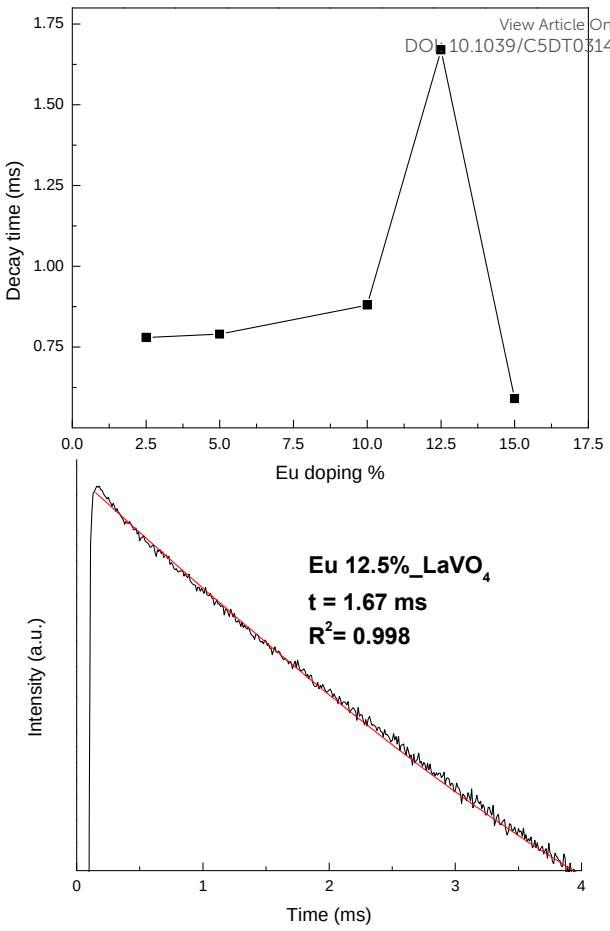

Fig. 9 Top: graph presenting the luminescence lifetime values of the 2.5%-15%Eu:$LaVO_4$ doped materials. Bottom: luminescence decay curve for 12.5%Eu:$LaVO_4$ sample. The red line represents the fitting result.

increases with the increase in doping percentage, where 12.5%Eu:$LaVO_4$ shows the highest intensity. The 15%Eu:$LaVO_4$ sample shows a drop in the emission intensity most likely due to concentration quenching. The increase of doping concentration also has an influence on the luminescence lifetime. The highest decay time was observed for the 12.5%Eu:$LaVO_4$ and was 1.67 ms (see Fig. 9 and Table 2). The absolute QY of the 12.5%Eu:$LaVO_4$ was determined to be 6%. For most known Eu^{3+} doped materials (e.g. Eu:YVO_4, Eu:Y_2O_3) the quenching concentration is around 5%. For our $LaVO_4$ materials the quenching concentration was observed only for the 15% Eu doping. This has been previously observed for other materials at the nano-size. It has been suggested that this can be caused in nano-sized materials by the deficiency of traps, which is a result of the limited primitive cells per particle, as well as the hindrance of energy transfer from the particle boundaries.[17,29]

Fig. 10 presents the high-resolution emission spectra of the 2.5% - 15% Eu:$LaVO_4$ samples. The spectra have been zoomed in to show the $^5D_0 \rightarrow {}^7F_0$, $^5D_0 \rightarrow {}^7F_1$, $^5D_0 \rightarrow {}^7F_2$ transition peaks to compare the site symmetry of the $LaVO_4$ material with different Eu^{3+} co-doping. For all of the samples with different Eu^{3+} doping percentages the positions of the transition peaks

are very similar. In monoclinic $LaVO_4$ there is only one La^{3+} site, therefore we would expect to see one $^5D_0 \rightarrow {}^7F_0$ peak. In all our Eu:$LaVO_4$ samples we observe a broadening of the $^5D_0 \rightarrow {}^7F_0$ peak. This can most likely be caused by the fact that in nano-sized particles we have Eu^{3+} ions occupying two types of sites – at (or near) the surface as well as in the interior of the particles. Therefore this can be the reason for the broadening of the $^5D_0 \rightarrow {}^7F_0$ transition peak. The $^5D_0 \rightarrow {}^7F_1$ peak is split three times suggesting the presence of a Eu^{3+} crystallographic site with low symmetry. For the 2.5%, 5%, 10% and 15% Eu:$LaVO_4$ samples the $^5D_0 \rightarrow {}^7F_2$ transition peak is split three times. In the 15%Eu:$LaVO_4$ sample some slight changes in the spectral splitting of this peak are observed. These changes can perhaps be due to a larger amount of Eu^{3+} ions lying at the surface of the particles (with Eu^{3+} doping the particle morphology was observed to change).

The luminescence lifetime and quantum yield values of several monoclinic and tetragonal Eu:$LaVO_4$ particles have previously been reported in literature. For example, for monoclinic 12%Eu:$LaVO_4$ nanorods a QY of 19% was reported. For tetragonal 10%Eu:$LaVO_4$ nanoparticles a QY of 65% was obtained. Both the nanorods and nanoparticles were prepared in a hydrothermal synthesis in the presence of either citric acid or EDTA.[17] For irregular nano-sized monoclinic 7%Eu:$LaVO_4$ particles obtained at 140 °C in a flask reaction in the presence of ethylene glycol a decay time of 0.632 ms was reported.[20] The luminescence lifetime decreased with further increase of Eu^{3+} ion concentration. As can be seen the luminescence properties of the previously reported Eu:$LaVO_4$ particles vary from those we observed during our study. This can most likely be explained by the differences in their shape and size. It is a known fact that in lanthanide doped materials the modification of a material's size and shape influences the emission spectra, luminescence lifetime, quantum yield and concentration quenching. Most of these changes can be linked to the structure distortions and surface defects caused by size/shape modification.[6]

As the 12.5%Eu:$LaVO_4$ sample showed the strongest emission intensity and longest decay time it was chosen for further co-doping with Y^{3+}, Gd^{3+} and Lu^{3+} in an attempt to increase its luminescence properties.

3.2.2. Photoluminescence properties of 12.5% Eu:$LaVO_4$ co-doped with Y^{3+}, Gd^{3+} and Lu^{3+} ions

The 12.5%Eu:$LaVO_4$ material was additionally co-doped with 2%, 5% and 10% of Y^{3+}, Gd^{3+} and Lu^{3+} ions. We have previously observed for Ln:Y_2WO_6 materials that additionally co-doping it with different concentrations of Gd^{3+} ions could drastically improve the luminescence properties.[30] The reason for the improvement of luminescence properties of the Ln:Y_2WO_6 materials after co-doping with Gd^{3+} ions is still not very clear. It was assumed that the presence of the Gd^{3+} ions in the material increases the luminescence properties because Gd^{3+} ions have better matching energy levels to accept the energy from the matrix material and subsequently pass it on to the luminescent Ln^{3+} ions. Also it is possible that the increase in luminescence properties was due to the change of local crystal field of the Ln^{3+} ions after additional co-doping with Gd^{3+} ions. For this research we have additionally chosen spectroscopically silent Y^{3+} and Lu^{3+} ions. Doping percentages of 2%, 5%, and 10% were chosen. As can be seen in Fig. 11 for the 2% Gd^{3+}, Y^{3+} and Lu^{3+} co-doped materials an increase in the luminescence intensity was observed compared to the 12.5%Eu:$LaVO_4$ sample. The highest increase was observed for the Gd^{3+} co-doped sample, next the Y^{3+} co-doped sample and last a slight increase of luminescence intensity for the Lu^{3+} co-doping. For all three co-doping ions it was observed that with higher doping percentages the luminescence intensities increased. This has been presented in Fig. 12. Therefore for this material we can see that not only co-doping it with Gd^{3+} ions increases the luminescence intensity, but also co-doping with Y^{3+} and Lu^{3+} gives a similar outcome.

The luminescence lifetimes and QY values are presented in Table 2. Co-doping the material with additional RE^{3+} ions lead to an increase of the QY values (the higher the doping percentages, the higher the QYs). A different tendency was observed for the decay times of the co-doped materials. In all cases the decay times of the co-doped samples were lower than of the 12.5%Eu:$LaVO_4$ sample. With higher co-doping percentage the decay time dropped further to lower values. In the case of the 12.5%Eu_2%Lu:$LaVO_4$ material the highest lifetime of the co-doped samples was observed (determined as 1.45 ms). This is most likely due to the fact that Lu^{3+} ions are

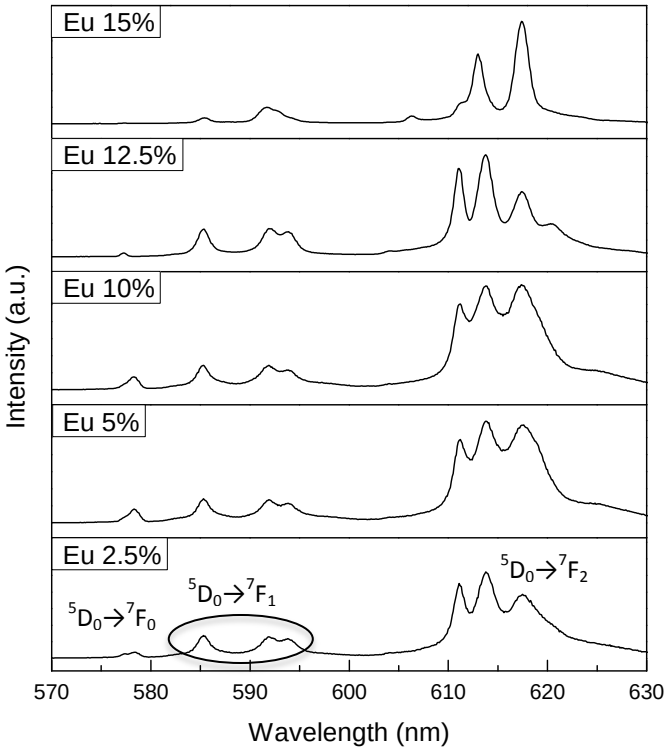

Fig. 10 High-resolution emission spectra of the $LaVO_4$ materials with different Eu^{3+} doping percentages.

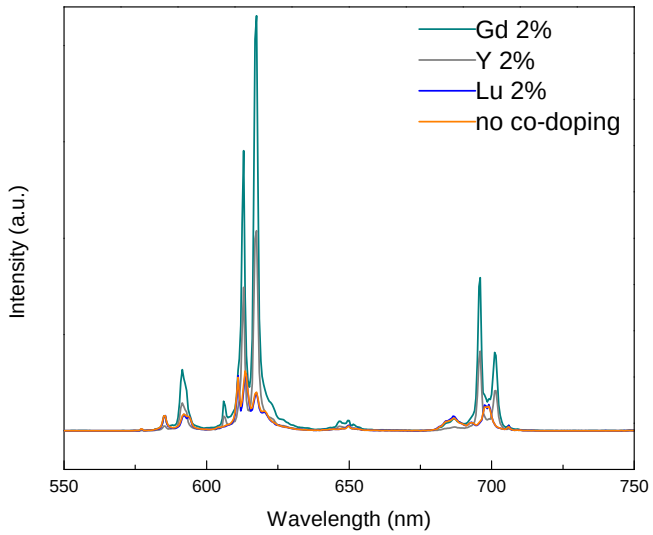

Fig. 11 Emission spectra of 12.5%Eu:$LaVO_4$ material compared with 12.5%Eu:$LaVO_4$ material co-doped with 2% Gd^{3+}, Y^{3+}, and Lu^{3+} ions.

the smallest of the three co-doped ions and at a low doping percentage of 2% does not have a significant influence on the material and therefore its luminescence value is similar to the one of the 12.5%Eu:$LaVO_4$ sample.

To further analyze this increase in luminescence the XRD patterns of Gd^{3+}, Y^{3+} and Lu^{3+} co-doped materials were analyzed in detail. Although up to a 15% doping of Eu^{3+} ions did not result in a mixture of the monoclinic and tetragonal phase, additionally co-doping the material yielded a mixture of the two phases. It was observed that for the different co-doped ions a different ratio of the monoclinic and tetragonal phase was obtained. Fig. S3 presents the XRD patterns at different Gd^{3+} co-doping percentages (the tetragonal peaks are labeled with a star). It can clearly be observed that with the increase of Gd^{3+} ions co-doped into the material the tetragonal phase becomes dominant in the material. Although a QY of 24% was obtained for this sample it is actually due to the presence of the tetragonal phase. At 10% Y^{3+} co-doping the tetragonal phase was also more dominant in the material than the monoclinic phase (see Fig. S4). Only for the Lu^{3+} co-doping even at 10% Lu^{3+} co-doping the monoclinic phase remains the dominantly present $LaVO_4$ phase in the material (see Fig. S5). Therefore from the analysis of the XRD patterns of the co-doped samples it is clear that the increase in the intensity and QY values is due to the presence of the tetragonal phase in the $LaVO_4$ materials. Fig. 13 presents the high-resolution emission spectra of the 12.5%Eu:$LaVO_4$ material with different Gd^{3+} co-doping percentages to get more insight into the site symmetry of the Eu^{3+} ions in the three materials with different Gd^{3+} co-doping percentages. The spectra have been zoomed in to show the $^5D_0 \rightarrow {}^7F_0$, $^5D_0 \rightarrow {}^7F_1$, $^5D_0 \rightarrow {}^7F_2$ transition peaks in greater detail. There are no significant differences in the relative intensities of the three transition peaks. Also the same amount of splittings of the peaks is observed indicating the same Eu^{3+} site symmetry in the case of 2%, 5% and 10% Gd^{3+} co-doping. Only some small changes in the relative intensities of the splittings are observed, this can be explained by the fact that

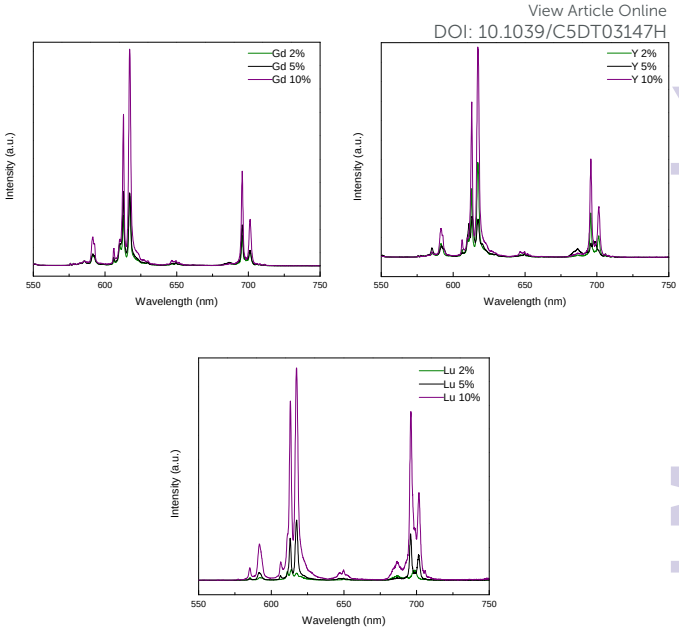

Fig. 12 Emission spectra of 12.5%Eu:$LaVO_4$ sample co-doped with 2%, 5%, and 10% Gd^{3+}, Y^{3+}, and Lu^{3+} ions.

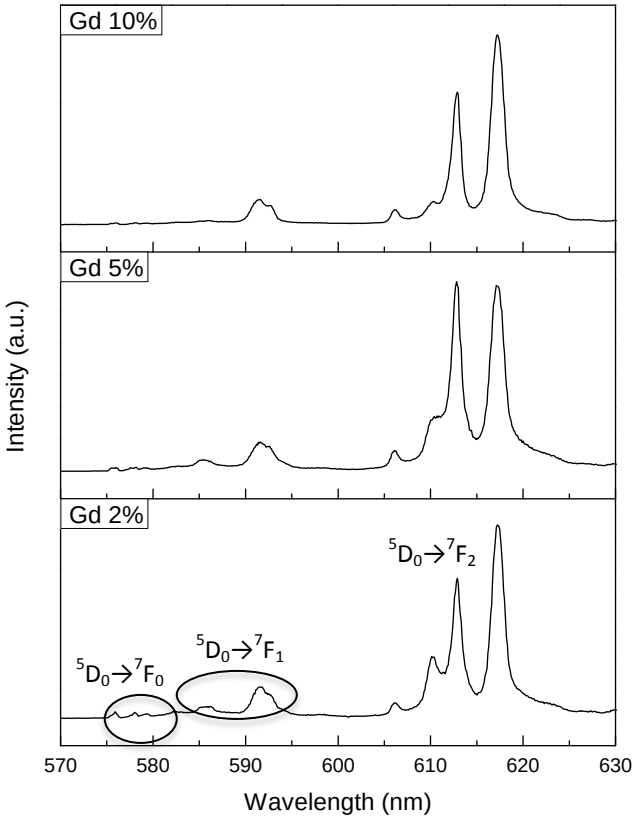

Fig. 13 High-resolution emission spectra of the 12.5%Eu:$LaVO_4$ materials with different Gd^{3+} co-doping percentages.

the ratio of the two crystallographic phases – monoclinic and tetragonal –changes with the co-doping percentage. What can be clearly noticed is a difference in the $^5D_0 \rightarrow {}^7F_0$ transition peak

for the Gd^{3+} co-doped materials compared to the 12.5%Eu:$LaVO_4$ material. Here there is more than one peak present indicating that there is more then one Eu^{3+} site (this seems logical considering that we have a mixture of two different $LaVO_4$ phases). The compiled high-resolution emission spectra of the 12.5%Eu:$LaVO_4$ material with different Y^{3+} and Lu^{3+} co-doping percentages have been presented in Fig. S13 and Fig. S14, respectively. In the 2% Lu^{3+} co-doped sample the $^5D_0 \rightarrow {}^7F_0$, $^5D_0 \rightarrow {}^7F_1$, $^5D_0 \rightarrow {}^7F_2$ transition peaks resemble those of the 12.5%Eu:$LaVO_4$ sample with no co-doping. In these cases this is due to the fact that the monoclinic $LaVO_4$ phase is dominantly present in the material. Higher co-doping percentages of Lu^{3+} (5% and 10%) as well as the Y^{3+} co-doped samples show a change in the relative peak intensities and splittings as well as additional peaks, which can be assigned to the $^5D_0 \rightarrow {}^7F_0$ transition. They resemble those of the Gd^{3+} co- doped samples, which have a higher percentage of the tetragonal phase.

The $LaVO_4$ nanoparticles form stable colloidal suspensions in water. The luminescence properties of the 12.5%Eu:$LaVO_4$ material and 12.5%Eu_10%Gd:$LaVO_4$ material (which showed the highest QY) were investigated in suspension (0.01 g of powder was suspended in 2 mL distilled water and kept in an ultrasound bath for 5 minutes). It was observed that there was no significant change in the shape of the emission spectrum and the values of the luminescence lifetimes before and after dispersion of the nanoparticles (Fig. S15-S17). Therefore this can lead to the conclusion that the particles do not encounter any modifications after dispersion in water. The colloidal suspension of the 12.5%Eu:$LaVO_4$ material and 12.5%Eu_10%Gd:$LaVO_4$ nanoparticles yielded strong red emission when placed under a laboratory lamp at an excitation wavelength of 302.0 nm (Fig. 14).

4. Conclusions

Here, we have presented the synthesis of nanosized Ln^{3+} doped $LaVO_4$ prepared in the presence of glycerol in a microwave assisted hydrothermal reaction. The synthesis requires a temperature of 180 °C and gives phase-pure materials after only 30 minutes. The obtained material showed a monoclinic $LaVO_4$ phase even after doping it with 15% Eu^{3+} ions. Detailed luminescence studies showed that the 12.5% Eu^{3+} doped sample showed the best properties (1.67 ms decay time and QY equal to 6%). It was further co-doped with Gd^{3+}, Y^{3+} and Lu^{3+} ions at different concentrations to investigate if the luminescence properties of these materials could be enhanced. It was observed that although the emission intensity and QYs increased with the co-doping of these ions a decrease of luminescence lifetime was observed for these samples. This can most likely be explained by the change in the radiative lifetime of the materials.

In our study we observed that the luminescence intensity and QYs of Eu^{3+} doped monoclinic $LaVO_4$ nanoparticles could be significantly increased with additional ion co-doping. More detailed investigation showed that this enhancement was most likely due to the presence of the tetragonal phase (unlike La^{3+} ions Gd^{3+}, Y^{3+} and Lu^{3+} have a preference to form the tetragonal $LnVO_4$ phase). Therefore the luminescence properties of the Eu:$LaVO_4$ material could be enhanced although this involved the additional presence of the tetragonal phase in the material. Due to the fact that these nano-sized particles form stable colloidal suspensions in water, which show strong luminescence emission intensity and decay times similar to those in powder form, they show potential for bioapplications (e.g. as biolabels) or for the formation of

Table 2 Decay times and quantum yields of the Eu:$LaVO_4$ samples and Gd^{3+}, Y^{3+}, Lu^{3+} co-doped samples (all values recorded for solid state samples).

View Article Online
DOI: 10.1039/C5DT03147H

Sample	Decay time [ms]	Quantum yield [%]
2.5%Eu:$LaVO_4$	0.78	-
5%Eu:$LaVO_4$	0.79	-
10%Eu:$LaVO_4$	0.88	-
12.5%Eu:$LaVO_4$	1.67	6
15%Eu:$LaVO_4$	0.59	-
12.5%Eu_2%Gd:$LaVO_4$	0.52	13
12.5%Eu_5%Gd:$LaVO_4$	0.52	14
12.5%Eu_10%Gd:$LaVO_4$	0.45	24
12.5%Eu_2%Y:$LaVO_4$	0.48	8
12.5%Eu_5%Y:$LaVO_4$	0.45	9
12.5%Eu_10%Y:$LaVO_4$	0.43	18
12.5%Eu_2%Lu:$LaVO_4$	1.45	6
12.5%Eu_5%Lu:$LaVO_4$	0.54	7
12.5%Eu_10%Lu:$LaVO_4$	0.51	13

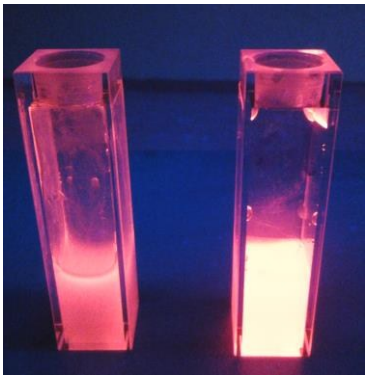

Fig. 14 Photo of water suspensions of 12.5%Eu:$LaVO_4$ sample (left) and 12.5%Eu_10%Gd:$LaVO_4$ sample (right) when placed under a laboratory UV lamp (302.0 nm excitation wavelength).

luminescent inks, which could be used to print luminescent films on various substrates.

Acknowledgements

RVD and IVD thank the Hercules Foundation (project AUGE/09/024 “Advanced Luminescence Setup”). KVH and RVD thank the Hercules Foundation (project AUGE/11/029 "3D-SPACE: 3D Structural Platform Aiming for Chemical Excellence"). KVH acknowledges the Research Fund – Flanders (FWO) for funding. IVD thanks Ghent University (project BOFGOA2015000302) for funding.

References

1 G. Liu and X. Chen, *Handbook on the Physics and Chemistry of Rare Earths*, K. A. Gschneidner Jr., J.-C. G Bünzli, V. K. Pecharsky, Elsevier Science: Amsterdam, 2007; Vol. 37, Chapter 233, pp. 99–169.
2 C.-H. Yan, Z.-G. Yan, Y.-P. Du, J. Shen, C. Zhang and W. Feng, *Handbook on the Physics and Chemistry of Rare Earths*, K. A. Gschneidner Jr., J.-C. G. Bünzli, V. K. Pecharsky, Elsevier Science: Amsterdam, 2011; Vol. 41, Chapter 251, pp. 275-472.
3 A. M. Kaczmarek**,** R. Van Deun, *Chem. Soc. Rev.,* **2013**, 42, 8835.
4 G. Blasse and B. C. Grabmaier, *Luminescent Materials*, Springer Verlag, Berlin, 1994.
5 *Phosphor Handbook*, ed. S. Shionoya and W. M. Yen, CRC Press, Boca Paton, 1999.
6 A. M. Kaczmarek, K. Van Hecke, R. Van Deun, *Chem. Soc. Rev.*, **2015**, 44, 2032.
7 J.-C. G. Bünzli, C. Piguet, *Chem. Soc. Rev*., **2005**, 34, 1048.
8 A. K. Levine, F. C. Palilla, *Appl. Phys. Lett*., **1964**, 5, 118.
9 Z. M. Fang, Q. Hong, Z. H. Zhou, S. J. Dai, W. Z. Weng, H. L. Wan, *Catal. Lett*., **1999,** 61, 39.
10 J. R. O’Connor, *Appl. Phys. Lett.,* **1966**, 9, 407.
11 R. C. Ropp, B. Carroll, *J. Inorg. Nucl. Chem.,* **1977**, 39, 1303.
12 H. Wu, H. Xu, Q. Su, T. Chen, M. Wu, *J. Mater. Chem.*, **2003**, 13, 1223.
13 S. Tang, M. Huang, F. Wang, F. Yu, G. Shang, J. Wu, *J. Alloys Compd.*, **2012**, 513, 474.
14 T. V. Gavrilović, D. J. Jovanović, V. Lojpur, M. D. Dramićanin, *Sci. Rep.*, **2014**, 4, 4209.
15 Q. Z. Dong, Y. H. Wang, L. L. Peng, H. J. Zhang, B. T. Liu, *Nanotechnology*, **2011**, 22, 215604.
16 Z. Huang, S. Huang, G. Ou, W. Pan, *Nanoscale*, **2012**, 4, 5065.
17 C.-J. Jia, L.-D. Sun, Z.-G. Yan, Y.-C. Pang, S.-Z. Lu, C.-H. Yan, *Eur. J. Inorg. Chem*., **2010**, 2626.
18 Q. Wang, Z. Zhang, Y. Zheng, W. Cai, Y. Yu, *CrystEngComm*, **2012**, 14, 4786.
19 J. Liu, Y. Li, *J. Mater. Chem.*, **2007**, 17, 1797.
20 R. Okram, N. R. Singh, Ak. M. Singh, *Micro Nano Lett*., **2011**, 6, 165.
21 C. E. Rice, W. R. Robinson*, Acta Crystallogr., Sect. B*, **1976**, 32, 2232.
22 H. Fuess, A. Kalllel, *J. Solid State Chem*., **1994**, 109, 197.
23 K. Binnemans, P. T. Jones, K. Van Acker, B. Blanpain, B. Mishra, D. Apelian, *JOM*, **2013**, 65, 846.
24 C.F. Macrae, I. J. Bruno, J. A. Chisholm, P. R. Edington, P. McCabe, E. Pidcock, L. Rodriguez-Monge, R. Taylor, J. van de Streek, P. A. Wood, *J. Appl. Cryst*., **2008**, 41, 466.
25 A. M. Pires, M. F. Santos, M. R. Davalos, E. B. Stucchi, *J. Alloys Compd*., **2002**, 344, 276.
26 Y.I. Pazura, V. N. Baumer, T. G. Deyneke, O. M. Vovk, R. P. Yavetskiy, *Funct. Mater*., **2010**, 17, 107.
27 M. Pal, U. Pal, J. M. G. Y. Jimenez, F. Perez-Rodriguez, *Nanoscale Res. Lett.*, **2012**, 7, 1.
28 X. Liu, L. Li, H. M. Noh, B. K. Moon, B. C. Choi, J. H. Jeong, *Dalton Trans.*, **2014**, 43, 8814.
29 Z. G. Wei, L. D. Sun, C. S. Liao, J. L. Yin, X. C. Jiang, C. H. Yan, S. Z. Lu, *J. Phys. Chem. B*, **2002**, 106, 10610.
30 A. M. Kaczmarek, K. Van Hecke, R. Van Deun, *Inorg. Chem*., **2014**, 53, 9498.